CLINICAL REPORT

AMERICAN JOURNAL OF medical genetics PART A

Severe Craniosynostosis With Noonan Syndrome Phenotype Associated With *SHOC2* Mutation: Clinical Evidence of Crosslink Between FGFR and RAS Signaling Pathways

Toshiki Takenouchi,[1] Yoshiaki Sakamoto,[2] Tomoru Miwa,[3] Chiharu Torii,[4] Rika Kosaki,[5] Kazuo Kishi,[2] Takao Takahashi,[1] and Kenjiro Kosaki[4]*

[1]Department of Pediatrics, Keio University School of Medicine, Tokyo, Japan

[2]Department of Plastic and Reconstructive Surgery, Keio University School of Medicine, Tokyo, Japan

[3]Department of Neurosurgery, Keio University School of Medicine, Tokyo, Japan

[4]Center for Medical Genetics, Keio University School of Medicine, Tokyo, Japan

[5]Division of Medical Genetics, National Center for Child Health and Development, Tokyo, Japan

Manuscript Received: 22 December 2013; Manuscript Accepted: 22 May 2014

Dysregulation in the RAS signaling cascade results in a family of malformation syndromes called RASopathies. Meanwhile, alterations in FGFR signaling cascade are responsible for various syndromic forms of craniosynostosis. In general, the phenotypic spectra of RASopathies and craniosynostosis syndromes do not overlap. Recently, however, mutations in ERF, a downstream molecule of the RAS signaling cascade, have been identified as a cause of complex craniosynostosis, suggesting that the RAS and FGFR signaling pathways can interact in the pathogenesis of malformation syndromes. Here, we document a boy with short stature, developmental delay, and severe craniosynostosis involving right coronal, bilateral lambdoid, and sagittal sutures with a de novo mutation in exon1 of *SHOC2* (c.4A > G p.Ser2Gly). This observation further supports the existence of a crosslink between the RAS signaling cascade and craniosynostosis. In retrospect, the propositus had physical features suggestive of a dysregulated RAS signaling cascade, such as fetal pleural effusion, fetal hydrops, and atrial tachycardia. In addition to an abnormal cranial shape, which has been reported for this specific mutation, craniosynostosis might be a novel associated phenotype. In conclusion, the phenotypic combination of severe craniosynostosis and RASopathy features observed in the propositus suggests an interaction between the RAS and FGFR signaling cascades. Patients with craniosynostosis in combination with any RASopathy feature may require mutation screening for molecules in the FGFR-RAS signaling cascade.

Key words: craniosynostosis; RAS; FGFR; *SHOC2*

How to Cite this Article:
Takenouchi T, Sakamoto Y, Miwa T, Torii C, Kosaki R, Kishi K, Takahashi T, Kosaki K. 2014. Severe craniosynostosis with noonan syndrome phenotype associated with *SHOC2* mutation: Clinical evidence of crosslink between FGFR and RAS signaling pathways.
Am J Med Genet Part A 164A:2869–2872.

INTRODUCTION

Deregulation in a single signaling cascade can lead to a relatively specific family of malformation syndromes. Disorders caused by a dysregulated RAS signaling are collectively called "RASopathies". Within the RASopathy family, combinations of distinct phenotypes (including short stature, characteristic facial features, cutaneous lesions, and congenital heart disease) and the types of mutated molecules define specific disease entities such as Noonan, cardio-facio-cutaneous, and Costello syndrome. The causative genes include *PTPN11*, *SOS1*, *RAF1*, *BRAF*, *HRAS*, *NRAS*, *CBL*, *MAP2K1*, *MAP2K2*, *NF1*, *SPRED1*, *SHOC2*, and *KRAS* [Viskochil, 2011].

The dysregulated FGFR signaling cascade results in various syndromic forms of craniosynostosis [Cohen, 2000]. Specific disease entities including Apert, Pfeiffer, Muenke, and Crouzon

Grant sponsor: Research on Applying Health Technology from the Ministry of Health, Labour and Welfare, Japan; Grant number: H23-013.
*Correspondence to:
Kenjiro Kosaki, M.D., Center for Medical Genetics, Keio University School of Medicine, 35 Shinanomachi, Shinjuku-ku, Tokyo 160-8582, Japan. E-mail: kkosaki@z3.keio.jp
Article first published online in Wiley Online Library (wileyonlinelibrary.com): 13 August 2014
DOI 10.1002/ajmg.a.36705

syndromes are defined according to the presence of physical defects other than defects of the cranial bones, such as limb anomalies. All these syndromes are caused by mutations in *FGFR* genes [Agochukwu et al., 2012]. *FGFR2* is regulated by *TWIST1*, which is a negative regulator of the master switch gene, *RUNX2* [Yousfi et al., 2002; Guenou et al., 2005]. *TWIST1* controls osteoblast differentiation [Ducy et al., 1997; Komori et al., 1997]. Mutations in *TWIST1* lead to Saethre–Chotzen syndrome [el Ghouzzi et al., 1997; Howard et al., 1997], whereas mutations in TCF12, a cofactor of TWIST1, lead to coronal craniosynostosis [Sharma et al., 2013].

Generally speaking, the phenotypic spectra of RASopathies and craniosynostosis syndromes do not overlap. In other words, they are thought to be independent from a dysmorphology standpoint. Recently, however, a reduced dosage of ERF 1/2 was discovered to cause complex craniosynostosis, suggesting that the RAS and FGFR signaling pathways can interact in the pathogenesis of malformation syndromes [Twigg et al., 2013]. The association between the RAS and FGFR2 pathways in the pathogenesis of craniosynostosis has been demonstrated in model organisms [Kim et al., 2003; Shukla et al., 2007]. Here, we document a boy with a mutation in *SHOC2* who presented with severe craniosynotosis, i.e., bilateral lambdoid, unilateral coronal and sagittal synostosis.

CLINICAL REPORT

The propositus was the first child of parents with no family history of an inherited genetic condition. The conception was achieved naturally. At 18 weeks of gestation, the propositus was noted to have left pleural effusion, which resolved spontaneously. He also had fetal hydrops. The propositus was born at 37 weeks of gestation via cesarean because of a breech position. The Apgar scores were 4 and 8 at 1 and 5 min, respectively. The birth weight was 2512 g (−0.4 SD), his length was 45 cm (−1.0 SD), and his OFC was 35.5 cm (+2.1 SD). He had respiratory distress with tachypnea and intercostal retractions, which improved with nasal directional positive airway pressure in combination with supplemental oxygen and diuretics. An echocardiogram showed a patent ductus arteriosus and a patent foramen ovale. He had atrial tachycardia, which was treated with propranolol. He was noted to have an abnormal head shape and the characteristic facial features of hypertelorism, protrusion of the nasal bridge, a U-shaped upper lip vermilion, and micrognathia. Karyotyping was performed, with a normal result of 46, XY.

Because of poor weight gain, he required tube feeding until 9 months of age. At 1 year and 2 months, his weight was 6640 g (−3.2 SD), his height was 65.4 cm (−4.4 SD), and OFC was 46 cm (−0.7 SD). His psychomotor development was delayed. He rolled over at 1 year 10 months, and he sat at 1 year 11 months. He did not have seizures or developmental regression.

At the age of 2 years 3 months, the propositus was referred to us because of his increased head circumference and progressive cranial deformity. His weight was 8.6 kg (−2.7 SD), height was 76 cm (−3.3 SD), and OFC was 49 cm (+0.07 SD). Upon examination, he had markedly asymmetric cranial shape and macrocephaly with a wide-open and bulging anterior fontanelle (Fig. 1). A funduscopic examination did not show papilledema. A head computed tomography scan with three-dimensional reconstruction showed a wide-open anterior fontanelle with craniosynostosis involving the right coronal suture, sagittal and bilateral lambdoid sutures, compatible with bilateral lambdoid and sagittal synostosis [Hing et al., 2009] (Fig. 2). Magnetic resonance imaging of the brain showed ventriculomegaly and a hypoplastic corpus callosum. Subsequently, the

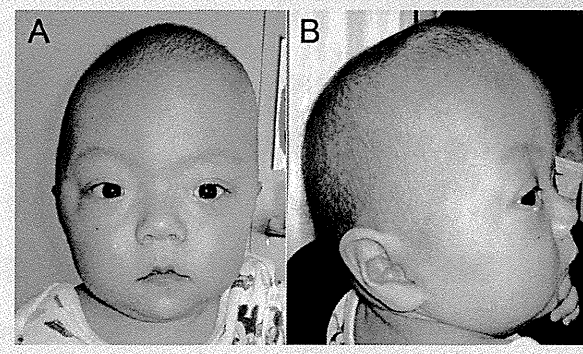

Figure 1. Facial features in the propositus. Frontal (A) and lateral (B) views of the propositus' facial photographs. Note markedly asymmetric cranial shape and macrocephaly with bulging anterior fontanelle, loose hair, and hypertelorism.

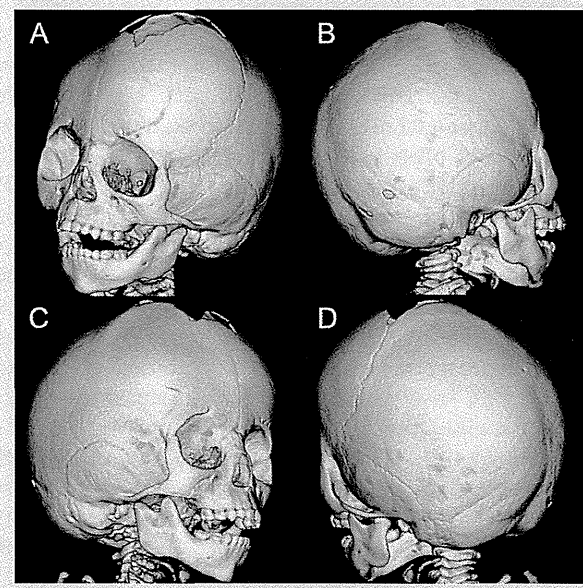

Figure 2. A cranial computed tomography with three-dimensional reconstruction demonstrating bilateral lambdoid and sagittal synostosis. Note wide-open anterior fontanelle (A), and craniosynostosis involving the right coronal suture (B and C), sagittal suture, and bilateral lambdoid sutures(B and D), compatible with bilateral lambdoid and sagittal synostosis.

propositus underwent a cranioplasty without major surgical complications.

MOLECULAR ANALYSIS

A local institutional review board approved the research protocol. A written consent was obtained from the parents for the molecular analysis. Genomic DNA was extracted from a peripheral blood sample of the propositus and his parents. The biological relationship between the propositus and his parents was confirmed using multiple microsatellite markers, including D1S189, D2S1388, D3S1744, D4S2366, D19S433, and D20S917. A custom-designed mutation analysis panel (SureSelect XT-Auto custom; Agilent Technologies, Santa Clara, CA) was run on a next-generation sequencer (MiSeq; Illumina, Inc., San Diego, CA). The list of genes on this panel comprises most of the causative genes listed in the classic textbook of dysmorphology: Smith's Recognizable Patterns of Human Malformation [Jones, 2006] (the list of genes is available upon request), including major components in the RAS/MAPK signaling cascade, i.e., *NF1*, *PTPN11*, *SOS1*, *RAF1*, *SPRED1*, and *SHOC2* [Takenouchi et al., 2013; Takenouchi et al., 2014]. After we aligned the sequencing reads to the reference human genome sequence (hs37d5) using BWA [Li and Durbin, 2009], local realignment around indels and base quality score recalibration were performed using Genome Analysis Toolkit software [McKenna et al., 2010]. Duplicate reads were removed using Picard (http://picard.sourceforge.net). Sequencing of the PCR products identified a de novo mutation in exon1 of *SHOC2* (NM_007373), c.4A > G p.Ser2Gly in the propositus. The same mutation has been reported as a cause of the Noonan syndrome phenotype [Cordeddu et al., 2009; Gripp et al., 2013]. We confirmed the result using Sanger sequencing with the following primers (forward: ATGATCAGAAATGGGCATAGTG, reverse: GGAGTCCTTCTTTCCATCTTTG). We further screened 4,813 genes associated with known human disease phenotypes using the TruSight One Sequencing Panel (Illumina, San Diego, CA) and found no additional pathogenic mutation in genes responsible for RASopathies or craniosynostosis syndromes. The panel covers all of the causative genes registered in the human gene mutation database (HGMD professional).

DISCUSSION

Here, we present a boy with severe craniosynostosis involving right coronal, bilateral lambdoid, and sagittal sutures with a de novo mutation in *SHOC2*. The present observation further supports the causal relationship between the RAS signaling cascade and craniosynostosis from molecular and clinical perspectives. In reviewing the literature, craniosynostosis appears to be rare among patients with mutations in the RASopathy genes, only *KRAS* mutations have been reported in four patients [Brasil et al., 2012; Kratz et al., 2009; Schubbert et al., 2006]. The observation that craniosynostosis and RASopathy phenotypes occurred as result of mutations in two different molecules each belonging to a single signaling cascade, i.e., SHOC2 and KRAS, further supports a crosslink between FGFR and RAS pathways.

Because of the severe craniosynostosis in the propositus, Noonan-like facial features were masked, leading to the exclusion of RASopathies from the differential diagnosis. However, in retrospect, the propositus had physical features suggestive of a dysregulated RAS signaling cascade, such as short stature, fetal pleural effusion, fetal hydrops, and atrial tachycardia. Similar cases may have escaped clinical recognition. Craniosynostosis in combination with RASopathy features may suggest a need for the mutation screening of molecules in the RAS signaling cascade.

The mutation identified in the propositus, i.e., c.4A > G p.Ser2Gly, is the same as a previously reported causative mutation for Noonan-like syndrome with loose anagen hair [Cordeddu et al., 2009]. Although the original paper did not mention the cranial shape of the affected individuals, subsequent reports have mentioned an abnormal head shape as a feature associated with this recurrent *SHOC2* mutation [Gripp et al., 2013]. Whether craniosynostosis is a feature associated with this *SHOC2* mutation warrants further investigation. The propositus in the present study may carry mutation(s) in gene(s) other than *SHOC2* that are responsible for the craniosynostosis. However, we did not find mutations in the genes known to be associated with craniosynostosis after performing an extensive mutation analysis.

In conclusion, the phenotypic combination of severe craniosynostosis and the RASopathy features observed in the propositus suggests an interaction between the RAS and FGFR signaling cascades. Patients with craniosynostosis in combination with RASopathy feature may require mutation screening of molecules in the FGFR-RAS signaling cascade.

ACKNOWLEDGMENT

We thank Namiko Saito and Yumi Obayashi for their technical assistance in the preparation of this article.

REFERENCES

Agochukwu NB, Solomon BD, Muenke M. 2012. Impact of genetics on the diagnosis and clinical management of syndromic craniosynostoses. Childs Nerv Syst 28:1447–1463.

Brasil AS, Malaquias AC, Kim CA, Krieger JE, Jorge AA, Pereira AC, Bertola DR. 2012. KRAS gene mutations in Noonan syndrome familial cases cluster in the vicinity of the switch II region of the G-domain: Report of another family with metopic craniosynostosis. Am J Med Genet A 158A:1178–1184.

Cohen MM Jr. 2000. Other Syndromes with Craniosynostosis. In: Cohen MM Jr, MacLean RE, editors Craniosynostosis diagnosis, evaluation, and management. Second ed. New York, NY: Oxford University Press, Inc. p. 1–199.

Cordeddu V, Di Schiavi E, Pennacchio LA, Ma'ayan A, Sarkozy A, Fodale V, Cecchetti S, Cardinale A, Martin J, Schackwitz W, Lipzen A, Zampino G, Mazzanti L, Digilio MC, Martinelli S, Flex E, Lepri F, Bartholdi D, Kutsche K, Ferrero GB, Anichini C, Selicorni A, Rossi C, Tenconi R, Zenker M, Merlo D, Dallapiccola B, Iyengar R, Bazzicalupo P, Gelb BD, Tartaglia M. 2009. Mutation of SHOC2 promotes aberrant protein N-myristoylation and causes Noonan-like syndrome with loose anagen hair. Nat Genet 41:1022–1026.

Ducy P, Zhang R, Geoffroy V, Ridall AL, Karsenty G. 1997. Osf2/Cbfa1: A transcriptional activator of osteoblast differentiation. Cell 89:747–754.

el Ghouzzi V, Le Merrer M, Perrin-Schmitt F, Lajeunie E, Benit P, Renier D, Bourgeois P, Bolcato-Bellemin AL, Munnich A, Bonaventure J. 1997.

Mutations of the TWIST gene in the Saethre–Chotzen syndrome. Nat Genet 15:42–46.

Gripp KW, Zand DJ, Demmer L, Anderson CE, Dobyns WB, Zackai EH, Denenberg E, Jenny K, Stabley DL, Sol-Church K. 2013. Expanding the SHOC2 mutation associated phenotype of Noonan syndrome with loose anagen hair: Structural brain anomalies and myelofibrosis. Am J Med Genet A 161:2420–2430.

Guenou H, Kaabeche K, Mee SL, Marie PJ. 2005. A role for fibroblast growth factor receptor-2 in the altered osteoblast phenotype induced by Twist haploinsufficiency in the Saethre–Chotzen syndrome. Hum Mol Genet 14:1429–1439.

Hing AV, Click ES, Holder U, Seto ML, Vessey K, Gruss J, Hopper R, Cunningham ML. 2009. Bilateral lambdoid and sagittal synostosis (BLSS): A unique craniosynostosis syndrome or predictable craniofacial phenotype? Am J Med Genet A 149A:1024–1032.

Howard TD, Paznekas WA, Green ED, Chiang LC, Ma N, Ortiz deLuna, Garcia RI, Delgado C, Gonzalez-Ramos M, Kline AD, Jabs EW. 1997. Mutations in TWIST, a basic helix-loop-helix transcription factor, in Saethre–Chotzen syndrome. Nat Genet 15:36–41.

Jones KL. 2006. Smith's recognizable patterns of human malformation. Philadelphia, PA: Elsevier, Saunders. p. 1–761.

Kim HJ, Lee MH, Park HS, Park MH, Lee SW, Kim SY, Choi JY, Shin HI, Kim HJ, Ryoo HM. 2003. Erk pathway and activator protein 1 play crucial roles in FGF2-stimulated premature cranial suture closure. Dev Dyn 227:335–346.

Komori T, Yagi H, Nomura S, Yamaguchi A, Sasaki K, Deguchi K, Shimizu Y, Bronson RT, Gao YH, Inada M, Sato M, Okamoto R, Kitamura Y, Yoshiki S, Kishimoto T. 1997. Targeted disruption of Cbfa1 results in a complete lack of bone formation owing to maturational arrest of osteoblasts. Cell 89:755–764.

Kratz CP, Zampino G, Kriek M, Kant SG, Leoni C, Pantaleoni F, Oudesluys-Murphy AM, Di Rocco C, Kloska SP, Tartaglia M, Zenker M. 2009. Craniosynostosis in patients with Noonan syndrome caused by germline KRAS mutations. Am J Med Genet A 149A:1036–1040.

Li H, Durbin R. 2009. Fast and accurate short read alignment with Burrows–Wheeler transform. Bioinformatics 25:1754–1760.

McKenna A, Hanna M, Banks E, Sivachenko A, Cibulskis K, Kernytsky A, Garimella K, Altshuler D, Gabriel S, Daly M, DePristo MA. 2010. The genome analysis toolkit: A MapReduce framework for analyzing next-generation DNA sequencing data. Genome Res 20:1297–1303.

Schubbert S, Zenker M, Rowe SL, Boll S, Klein C, Bollag G, van der Burgt I, Musante L, Kalscheuer V, Wehner LE, Nguyen H, West B, Zhang KY, Sistermans E, Rauch A, Niemeyer CM, Shannon K, Kratz CP. 2006. Germline KRAS mutations cause Noonan syndrome. Nat Genet 38:331–336.

Sharma VP, Fenwick AL, Brockop MS, McGowan SJ, Goos JA, Hoogeboom AJ, Brady AF, Jeelani NO, Lynch SA, Mulliken JB, Murray DJ, Phipps JM, Sweeney E, Tomkins SE, Wilson LC, Bennett S, Cornall RJ, Broxholme J, Kanapin A, Whole-Genome Sequences C, Johnson D, Wall SA, van der Spek PJ, Mathijssen IM, Maxson RE, Twigg SR, Wilkie AO. 2013. Mutations in TCF12, encoding a basic helix-loop-helix partner of TWIST1, are a frequent cause of coronal craniosynostosis. Nat Genet 45:304–307.

Shukla V, Coumoul X, Wang RH, Kim HS, Deng CX. 2007. RNA interference and inhibition of MEK-ERK signaling prevent abnormal skeletal phenotypes in a mouse model of craniosynostosis. Nat Genet 39:1145–1150.

Takenouchi T, Hida M, Sakamoto Y, Torii C, Kosaki R, Takahashi T, Kosaki K. 2013. Severe congenital lipodystrophy and a progeroid appearance: Mutation in the penultimate exon of FBN1 causing a recognizable phenotype. Am J Med Genet A 161:3057–3062.

Takenouchi T, Shimizu A, Torii C, Kosaki R, Takahashi T, Saya H, Kosaki K. 2014. Multiple cafe au lait spots in familial patients with MAP2K2 mutation. Am J Med Genet A 164:392–396.

Twigg SR, Vorgia E, McGowan SJ, Peraki I, Fenwick AL, Sharma VP, Allegra M, Zaragkoulias A, Sadighi Akha E, Knight SJ, Lord H, Lester T, Izatt L, Lampe AK, Mohammed SN, Stewart FJ, Verloes A, Wilson LC, Healy C, Sharpe PT, Hammond P, Hughes J, Taylor S, Johnson D, Wall SA, Mavrothalassitis G, Wilkie AO. 2013. Reduced dosage of ERF causes complex craniosynostosis in humans and mice and links ERK1/2 signaling to regulation of osteogenesis. Nat Genet 45:308–313.

Viskochil DH. 2011. Disorders of the ras pathway: An introduction. Am J Med Genet C Semin Med Genet 157:79–82.

Yousfi M, Lasmoles F, Marie PJ. 2002. TWIST inactivation reduces CBFA1/RUNX2 expression and DNA binding to the osteocalcin promoter in osteoblasts. Biochem Biophys Res Commun 297:641–644.

CLINICAL REPORT

AMERICAN JOURNAL OF medical genetics PART A

Porencephaly in a Fetus and HANAC in Her Father: Variable Expression of *COL4A1* Mutation

Toshiki Takenouchi,[1,2] Masaki Ohyagi,[3] Chiharu Torii,[2] Rika Kosaki,[4] Takao Takahashi,[1] and Kenjiro Kosaki[2]*

[1]Department of Pediatrics, Keio University School of Medicine, Tokyo, Japan

[2]Center for Medical Genetics, Keio University School of Medicine, Tokyo, Japan

[3]Department of Internal Medicine, Tokyo Metropolitan Bokutoh Hospital, Tokyo, Japan

[4]Division of Medical Genetics, National Center for Child Health and Development, Tokyo, Japan

Manuscript Received: 14 January 2014; Manuscript Accepted: 18 September 2014

COL4A1-associated disorders encompass a wide range of hereditary vasculopathy, including porencephaly and HANAC (adult-onset hemorrhagic stroke with cerebral aneurysm and retinal arterial tortuosity, renal cysts, and thenar muscle cramp). It remains elusive whether or not porencephaly and HANAC are molecularly distinctive disorders due to different classes of mutations. We report on a girl with porencephaly and an episode of microangiopathic hemolysis in infancy and her father with HANAC, both of whom had a heterozygous missense mutation of *COL4A1* (c.3715G>A, p.G1239R). The current observation implies phenotypic diversities of *COL4A1* mutations.

Key words: HANAC; COL4A1; Porencephaly

How to Cite this Article:
Takenouchi T, Ohyagi M, Torii C, Kosaki R, Takahashi T, Kosaki K. 2015. Porencephaly in a Fetus and HANAC in her father: Variable expression of *COL4A1* mutation.
Am J Med Genet Part A 167A:156–158.

INTRODUCTION

HANAC (hereditary angiopathy with nephropathy, aneurysms, and muscle cramps) [OMIM611773] is a recently established genetic condition characterized by cerebrovascular events and cerebral aneurysm formation, hematuria and cystic kidney disease, and retinal arterial tortuosity [Plaisier et al., 2007]. The mechanistic basis of this systemic vascular disorder is disruption of vascular wall integrity as a result of heterozygous *COL4A1* mutations. In the mean time, heterozygous *COL4A1* and *COL4A2* mutations have attracted attention as a cause of porencephaly due to prenatal cerebrovascular events [Gould et al., 2005; Gould et al., 2006; Plaisier et al., 2010; Yoneda et al., 2012]. It is known that *COL4A1* mutations are responsible for not only familial cases with porencephaly but also a substantial portion (i.e., 21%) of the sporadic cases [Yoneda et al., 2013]. Here, we report a family with a *COL4A1* mutation in which the father manifested with HANAC and his child with porencephaly.

CLINICAL REPORT

A female fetus was found to have intracranial hemorrhage with cystic changes on prenatal ultrasonography and magnetic resonance imaging (MRI) at 33 weeks of gestation (Fig. 1A,B). She was born at 35 weeks and 6 days of gestation by cesarean because of arrested fetal growth. Birth weight was 1878 grams (−1.5 SD), length was 42.6 cm (−1.4 SD), and head circumference was 29.6 cm (−1.6 SD). Physical examination at birth was unremarkable. A postnatal brain MRI showed porencephaly in the left hemisphere (Fig. 1C). She developed jaundice and anemia with evidence of intravascular hemolysis at age of 1 month, which was suggestive of microangiopathy. She later developed right hemiparesis at 12 months and seizure at 15 months of age. The combination of porencephaly and progressive hemolytic anemia led to a suspicion of basement membrane disease, and a *COL4A1* mutation analysis was performed.

Her father presented with a cerebrovascular event of adult onset, that is, sudden onset of transient left hemiparesis and difficulty in speaking, at age 38 years. He had the past history of microscopic hematuria and nephrotic syndrome. He also experienced muscle cramp in the left thumb while playing a videogame, which had

Conflict of interest: none

Abbreviations: HANAC, hereditary angiopathy with nephropathy, aneurysms, and muscle cramps; MRI, magnetic resonance imaging.

*Correspondence to:
Kenjiro Kosaki, M.D., Center for Medical Genetics, Keio University School of Medicine, 35 Shinanomachi, Shinjuku-ku, Tokyo, 160-8582, Japan.
E-mail: kkosaki@z3.keio.jp

Article first published online in Wiley Online Library (wileyonlinelibrary.com): 25 November 2014
DOI 10.1002/ajmg.a.36823

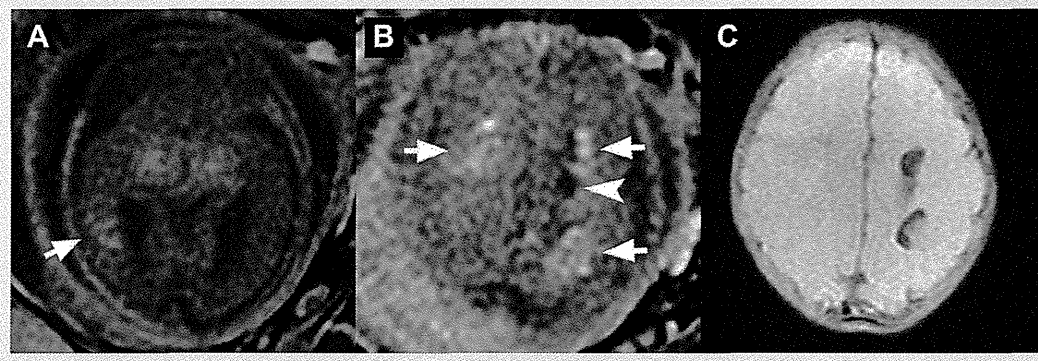

FIG. 1. Fetal and postnatal neuroimaging of the proposita. Fetal brain MRI obtained at 33 weeks of gestation (A and B) showing scattered T1 hyperintense lesions (arrows), likely representing hemorrhage, and a hypodensity suggestive of porencephaly (arrowhead). A postnatal brain MRI shows left hemispheric porencephaly (C).

started at the age 22 years, and lasted for one minute, causing significant disabilities in his everyday life. Creatinine kinase level was within the normal limits. Fundoscopic examination showed mild retinal arterial tortuosity. Renal ultrasound examination revealed small cysts measuring less than 5 mm. Brain MRI demonstrated extensive white matter lesions, multiple chronic hemorrhagic foci, and a cerebral arterial aneurysm at the left carotid siphon (Fig. 2). These vascular phenotypes were consistent with a diagnosis of HANAC.

MOLECULAR ANALYSIS

Genomic DNA was extracted from whole blood samples from the proposita and her parents. A mutation analysis panel (SureSelect XT-Auto custom; Agilent Technologies, Santa Clara, CA) was custom-designed to include major causative genes of congenital disorders primarily affecting the central nervous system, including *COL4A1* (the list of genes is available upon request). The sequencing of their PCR products using the panel and a next-generation sequencer (MiSeq; Illumina, Inc. San Diego, CA) identified a heterozygous missense mutation in exon 42 of *COL4A1* (NM_001845), that is, c.3715G>A p.Gly1239Arg in the proposita and her father, but not in her mother (Fig. 3). Sanger sequencing of the same PCR products confirmed the result (Fig. 3). The p.Gly1239Arg was not present in the dbSNP137, 1000 genomes Project (http://www.1000genomes.org/), ESP6500, or the Japanese SNP dataset of 1208 normal individuals (Human Genetic Variation Browser, http://www.genome.med-kyoto-u.ac.jp/SnpDB). Although there is no direct evidence of pathogenicity of this specific mutation, three different bioinformatics programs all predicted that the p.Gly1239Arg mutation in COL4A1 is

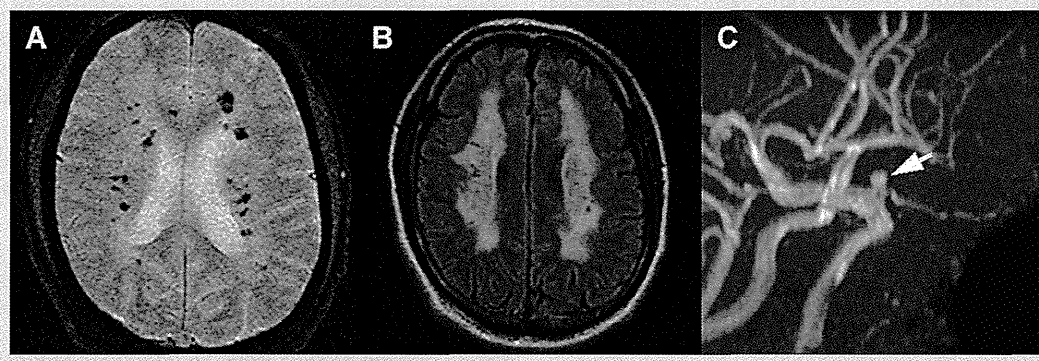

FIG. 2. Neuroimaging of the proposita's father. MRI of the brain showing scattered multiple hypodensities on T2* gradient echo imaging representing paramagnetic signals as a result of chronic hemorrhage (A) and a diffuse white matter lesion on a fluid-attenuated inversion recovery image (B). Magnetic resonance angiography shows a cerebral aneurysm at the left carotid siphon measuring approximately 3 mm (arrow, C). These radiographic features are compatible with a diagnosis of HANAC.

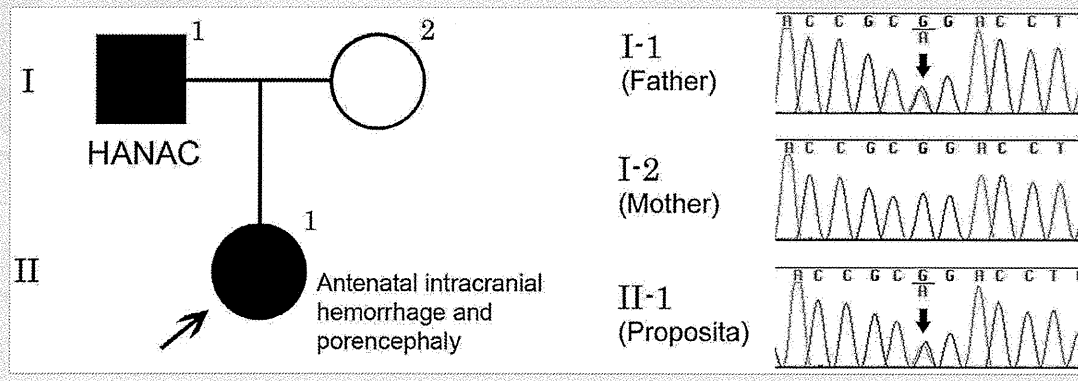

FIG. 3. Family pedigree and sequence chromatograms. The proposita had an antenatal intracranial hemorrhage, resulting in porencephaly. Her father had history of hematuria, an ischemic stroke at 38 years of age, cerebral aneurysm, and retinal arterial tortuosity, consistent with a diagnosis of HANAC. Sequence chromatograms shows that a single heterozygous nucleotide change, c.3715G>A, is present in the proposita (II-1) and her father (I-1), but not in her mother (I-2).

pathogenic (PolyPhen2, "probably damaging"; SIFT, "deleterious"; and MutationTaster, "disease-causing").

DISCUSSION

We reported on a familial case of porencephaly and hemolysis in a girl and HANAC in her father, who had a heterozygous mutation causing substitution of arginine for glycine in the triple helical region of COL4A1. The p.Gly1239Arg mutation was highly likely to be disease-causing. It is the rule that a single amino acid substitution for glycine residue in the triple helical region of a major collagen is pathogenic [Gupta et al., 1997; Nussbaum et al., 2007]. All mutations previously reported in HANAC were the same type of mutations [Plaisier et al., 2010]. Furthermore, it is known that a similar missense mutation (p.Gly1236Arg) is responsible for COL4A1-related vasculopathy [Gould et al., 2005].

Our observation suggested a significant variability in the expression of COL4A1-related basement membrane diseases. In autosomal dominant disorders, intrafamilial variability is the rule rather than the exception. From the clinical viewpoint; however, antenatal porencephaly and adult-onset HANAC are discrete conditions. Thus, we have to be careful in genetic counseling for COL4A1-associated disorders, in that a patient with a late-onset manifestation may have an affected child with a congenital phenotype, and vice versa.

ACKNOWLEDGMENTS

We thank Namiko Saito and Yumi Obayashi for their technical assistance in the preparation of this article.

FUNDING

This work was supported by Research Grants from the Ministry of Health, Labour and Welfare, Japan.

REFERENCES

Gould DB, Phalan FC, Breedveld GJ, van Mil SE, Smith RS, Schimenti JC, Aguglia U, van der Knaap MS, Heutink P, John SW. 2005. Mutations in Col4a1 cause perinatal cerebral hemorrhage and porencephaly. Science 308:1167–1171.

Gould DB, Phalan FC, van Mil SE, Sundberg JP, Vahedi K, Massin P, Bousser MG, Heutink P, Miner JH, Tournier-Lasserve E, John SW. 2006. Role of COL4A1 in small-vessel disease and hemorrhagic stroke. N Engl J Med 354:1489–1496.

Gupta MC, Graham PL, Kramer JM. 1997. Characterization of alpha1(IV) collagen mutations in Caenorhabditis elegans and the effects of alpha1 and alpha2(IV) mutations on type IV collagen distribution. J Cell Biol 137:1185–1196.

Nussbaum RL, McInnes RR, Willard HF, Hamosh A. 2007. Chapter 12 The molecular, biochemical, and cellular basis of genetic disease. Thompson & Thompson genetics in medicine [electronic resource]. Philadelphia: Saunders/Elsevier. p345–p392.

Plaisier E, Chen Z, Gekeler F, Benhassine S, Dahan K, Marro B, Alamowitch S, Paques M, Ronco P. 2010. Novel COL4A1 mutations associated with HANAC syndrome: A role for the triple helical CB3[IV] domain. Am J Med Genet Part A 152A:2550–2555.

Plaisier E, Gribouval O, Alamowitch S, Mougenot B, Prost C, Verpont MC, Marro B, Desmettre T, Cohen SY, Roullet E, Dracon M, Fardeau M, Van Agtmael T, Kerjaschki D, Antignac C, Ronco P. 2007. COL4A1 mutations and hereditary angiopathy, nephropathy, aneurysms, and muscle cramps. N Engl J Med 357:2687–2695.

Yoneda Y, Haginoya K, Arai H, Yamaoka S, Tsurusaki Y, Doi H, Miyake N, Yokochi K, Osaka H, Kato M, Matsumoto N, Saitsu H. 2012. De novo and inherited mutations in COL4A2, encoding the type IV collagen alpha2 chain cause porencephaly. Am J Hum Genet 90:86–90.

Yoneda Y, Haginoya K, Kato M, Osaka H, Yokochi K, Arai H, Kakita A, Yamamoto T, Otsuki Y, Shimizu S, Wada T, Koyama N, Mino Y, Kondo N, Takahashi S, Hirabayashi S, Takanashi J, Okumura A, Kumagai T, Hirai S, Nabetani M, Saitoh S, Hattori A, Yamasaki M, Kumakura A, Sugo Y, Nishiyama K, Miyatake S, Tsurusaki Y, Doi H, Miyake N, Matsumoto N, Saitsu H. 2013. Phenotypic spectrum of COL4A1 mutations: Porencephaly to schizencephaly. Ann Neurol 73:48–57.

Pediatric Neurology 52 (2015) 226–229

Contents lists available at ScienceDirect

Pediatric Neurology

journal homepage: www.elsevier.com/locate/pnu

Clinical Observations

Paramagnetic Signals in the Globus Pallidus as Late Radiographic Sign of Juvenile-Onset GM1 Gangliosidosis

Toshiki Takenouchi MD [a], Rika Kosaki MD [b], Kazuhiko Nakabayashi PhD [c], Kenichiro Hata MD [c], Takao Takahashi MD [a], Kenjiro Kosaki MD [d,*]

[a] *Department of Pediatrics, Keio University School of Medicine, Tokyo, Japan*
[b] *Division of Medical Genetics, National Center for Child Health and Development, Tokyo, Japan*
[c] *Department of Maternal-Fetal Biology, National Center for Child Health and Development, Tokyo, Japan*
[d] *Center for Medical Genetics, Keio University School of Medicine, Tokyo, Japan*

ABSTRACT

BACKGROUND: The juvenile form of GM1 gangliosidosis lacks specific physical findings and thus is often a diagnostic challenge for clinicians. T_2 hypodensity in the globus pallidus is a characteristic radiographic sign of neurodegeneration with iron accumulation in the brain that is observed in GM1 gangliosidosis, but the exact timing when this radiographic sign becomes apparent remains to be elucidated. **PATIENTS:** Two male siblings had normal development until 2 years of age and then developed psychomotor regression with dystonia. Their neuroimaging studies indicated progressive global cerebral atrophy. Exome sequencing identified compound heterozygous missense mutations in *GLB1*, leading to a diagnosis of GM1 gangliosidosis. **RESULTS:** A retrospective review of neuroimaging studies revealed that the two patients had strikingly similar clinical courses and radiographic progressions with cortical atrophy that preceded the T_2 hypointensity in the globus pallidus. **CONCLUSIONS:** Paramagnetic signals in the globus pallidus become apparent relatively late during the disease course, once cerebral atrophy has already become prominent. A comprehensive diagnostic approach involving clinical, radiographic, and genetic testing is necessary for the early identification of affected individuals.

Keywords: GM1 gangliosidosis, GLB1, neurodegeneration with brain iron accumulation, next-generation sequencing

Pediatr Neurol 2015; 52: 226-229

Introduction

GM1 gangliosidosis is a lysosomal disorder caused by a deficiency in β-galactosidase. This rare metabolic disorder is inherited in an autosomal recessive fashion and is characterized by neurodegeneration manifesting as psychomotor regression. Unlike its classic infantile form, which exhibits hepatosplenomegaly and macular cherry-red spots, the clinical presentation of the juvenile form of GM1 gangliosidosis (OMIM, 230600) lacks key diagnostic features.[1] In addition, the causative accumulated metabolite, GM1 ganglioside, cannot be identified using routine metabolic screenings, such as serum amino acid and urine organic acid profiling, making it highly challenging for clinicians to make a correct diagnosis.

Next-generation sequencing is a high-throughput DNA sequencing technology that is being increasingly used in many fields of medicine. In patients with undiagnosed neurological conditions, the diagnostic yield of exome sequencing is as high as 25%, suggesting the clinical utility of this approach.[2] Indeed, the first successful case in the National Institutes of Health-sponsored Undiagnosed Disease Program was a patient with undiagnosed juvenile-onset GM1 gangliosidosis whose genetic diagnosis was delineated using exome sequencing.[3]

In practice, almost all patients with neurological dysfunction undergo brain magnetic resonance imaging as the first line of testing before resorting to exome sequencing. The presence of paramagnetic signals in the basal ganglia,

Article History:
Received April 13, 2014; Accepted in final form September 13, 2014
* Communications should be addressed to: Dr. Kosaki; Center for Medical Genetics; Keio University School of Medicine; 35 Shinanomachi, Shinjuku-ku; Tokyo, 160-8582, Japan.
E-mail address: kkosaki@z3.keio.jp

0887-8994/$ - see front matter © 2015 Elsevier Inc. All rights reserved.
http://dx.doi.org/10.1016/j.pediatrneurol.2014.09.022

typically represented as T_2 hypodensity with T_1 hyperintensity, occurring in the setting of neurological deterioration points to a group of disorders termed "neurodegeneration with brain iron accumulation (NBIA)." The differential diagnosis of NBIA includes pantothenate kinase-associated neurodegeneration (NBIA1; OMIM, 234200), PLA2G6-associated neurodegeneration (NBIA2A; OMIM, 256600), mitochondrial membrane protein-associated neurodegeneration (NBIA4; OMIM, 614298), fatty-acid hydroxylase-associated neurodegeneration, Kufor-Rakeb syndrome (OMIM, 606693), GM1 gangliosidosis, and fucosidosis (OMIM, 230000). Thus the presence of T_2 hypointensities, representing iron deposition, in the globus pallidus is considered as a key radiographic sign of GM1 gangliosidosis.[4,5] However, the time window for the appearance of this radiographic sign has remained unknown.

Clinical descriptions

Patient 1

The propositus was born at 39 weeks of gestation via normal spontaneous vaginal delivery. His birth weight was 3170 g (+0.92 standard deviation [SD]), his height was 49.5 cm (+0.38 SD), and his head circumference was 35.5 cm (+1.7 SD). He sat at 6 months, crawled at 8 months, and stacked blocks at 10 months. At 12 months of age, he could stand up and walk with support.

Although, he walked independently at around 18 months of age, his gait was unsteady because of increased muscle tone. By 18 months of age, he stopped saying "bye-bye" or "hi" and became unable to stand up from a sitting position. At 2 years of age, his finger dexterity remained poor. He had normal brain magnetic resonance imaging findings and normal electroencephalogram and auditory brainstem responses. His motor and cognitive functions continued to deteriorate, and he exhibited a developmental quotient of 36 at age 3 years and 6 months. At 4 years of age, he started to have refractory epileptic seizures with multifocal spikes on an electroencephalogram.

At age 12 years, he was not communicative and exhibited continuous dystonic posturing requiring a wheelchair for locomotion. He had no overt physical deformity or hepatosplenomegaly, and his fundoscopic examination was normal. An extensive investigation, including karyotyping and urine organic acid and plasma amino acid profiling, produced only normal findings. Serial neuroimaging revealed progressive cerebral atrophy with an increasing T_2 hypodensity in the globi pallidi (Figure).

Patient 2

This boy was a younger sibling of Patient 1. He was born at 39 weeks of gestation via normal spontaneous vaginal delivery with no perinatal complications. His birth weight was 3230 g (+0.64 SD), and his head circumference was 34 cm (+0.57 SD). At one year of age, exhibited normal development and pointed to objects, said "Mama," and responded to his name. Around 18 months of age, he was observed to become easily tired and to have a "clumsy gait." His mother recalled that his motor function was best between 18 months and 2 years of age, and he had approximately 50 words. By the age of 2 years, his finger dexterity had worsened. By 3 years of age, he easily stumbled, fell, and required assistance walking. His speech deteriorated with reduced spontaneous speech and echolalia. His motor and cognitive functions progressed, and he barely walked with support and only had 10 words at 7 years of age. He developed refractory epileptic seizures. He had constant dystonia, equinus feet, frequent myoclonus, and Babinski signs. A neuroimaging study performed at age 9 years demonstrated global cerebral atrophy with T_2 hypodensity in the globi pallidi (Figure).

Molecular analysis

The local institutional review board approved the research protocol for the molecular studies. Informed consent was obtained from the parents. Whole exome sequencing[6] identified compound heterozygous missense mutations in exon5 and exon6 of *GLB1* (NM_000404.2), that are, c.520T>C p.Tyr174His and c.601C>T p.Arg201Cys, respectively. These results were confirmed using Sanger sequencing. The Arg201Cys mutation has been reported to be pathogenic in Japanese patients with GM1 gangliosidosis.[7] An enzyme assay of β-galactosidase in the peripheral blood indicated significantly reduced activities: 8.6 nmol/mg protein/h (Reference: 37.6-230.1) in Patient 1 and 10.7 nmol/mg protein/h in Patient 2.

Discussion

We describe brothers who presented with psychomotor regression and global cerebral atrophy with T_2 hypodensity in the globus pallidus. Through exome sequencing in quad, we identified a compound heterozygous mutation in *GLB1*. The enzymatic assay indicated reduced β-galactosidase activities in the affected siblings, confirming the diagnosis of juvenile-onset GM1 gangliosidosis.

The serial neuroimaging studies of the siblings exhibited a characteristic pattern of radiographic progressions. First, the two patients showed strikingly similar clinical courses and radiographic progressions. This high reproducibility between two siblings carrying the exact same *GLB1* mutation suggests a strong influence of genotype on the radiographic progression. Second, the basal ganglia lesions are a relatively late finding, occurring years after the onset of clinical regression and well after the onset of cortical atrophy. In the present family, at least, these lesions first appeared at around 7-8 years of age and then progressed. Because T_2 shortening representing iron deposition in the basal ganglia is considered to be abnormal if present in children less than 10 years of age,[8] the early emergence of a paramagnetic signal in the globus pallidus provides a diagnostic clue. However, the current observation that the paramagnetic signals became apparent relatively late during the disease course suggests that a radiographic approach alone is not sufficient for the early identification of patients.

The limitation of our observation is that the acquisition parameters and sequences were not exactly uniformed, although all images were obtained using long repetition time [TR] and long echo time [TE] sequences: fluid-attenuated inversion recovery image (TR = 7000-8802 ms, TE = 108-124 ms) or T_2-weighted image (TR = 3500 ms, TE = 91 ms). This was because each imaging study was obtained at different hospitals and imaging data were

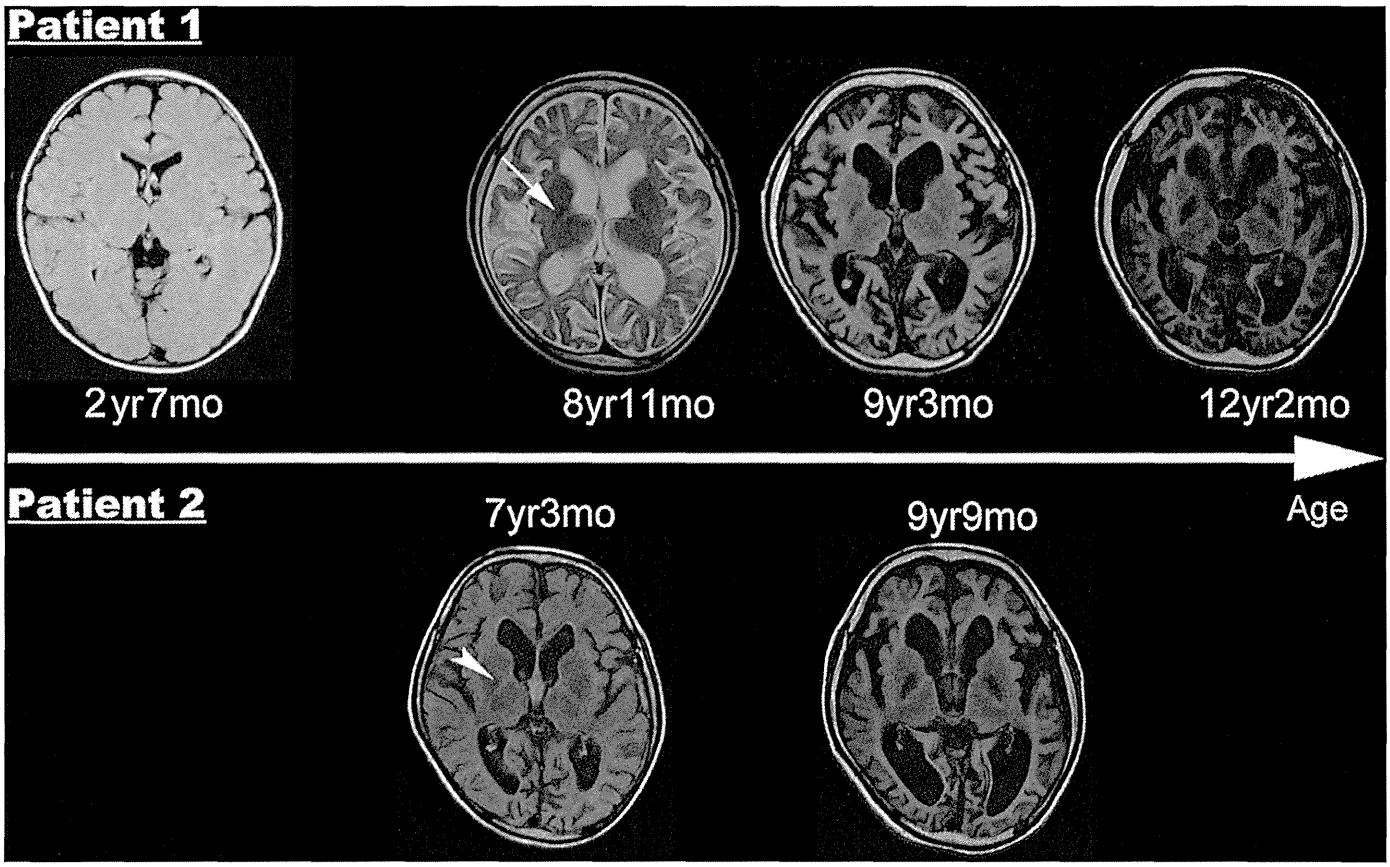

FIGURE.
Serial neuroimaging in Patients 1 and 2 reveal progressive diffuse cerebral atrophy. In Patient 1, fluid-attenuated inversion recovery (FLAIR) image (repetition time [TR] = 7000 ms, echo time [TE] = 110 ms) at age 2 years and 7 months was normal. A T_2-weighted image (TR = 3500 ms, TE = 91 ms) at 8 years 11 months revealed significant cerebral atrophy with barely noticeable hypointense signals in the globi pallidi (arrow). The cerebral atrophy and paramagnetic signals in the basal ganglia became more pronounced on the subsequent FLAIR images at 9 years 3 months (TR = 8802 ms, TE = 108 ms) and 12 years 2 months (TR = 8800 ms, TE = 124 ms). In Patient 2, a FLAIR image (TR = 8802 ms, TE = 108 ms) at 7 years 3 months revealed marked cerebral atrophy with minimal hypodensity in the globi pallidi (arrowhead). The cerebral atrophy and the paramagnetic signals became more apparent on the subsequent FLAIR image (TR = 8800 ms, TE = 124 ms) at 9 years 9 months.

collected retrospectively. Although it is difficult to delineate the exact time point when the basal ganglia lesion first appeared, it is clear that the basal ganglia lesions occurred years after the onset of cortical atrophy.

Early identification may be critical for therapeutic intervention in treatable neurodegenerative disorders. Several lysosomal disorders, such as Pompe disease, have become treatable with enzyme replacement therapy over the past few decades. Although no such definitive therapeutic option is currently available for GM1 gangliosidosis, the administration of a chemical chaperone, that is, N-octyl-4-epi-β-valienamine, in a mouse model of GM1 gangliosidosis increased β-galactosidase activity and prevented neurological deterioration.[9] Early diagnosis would thus be a prerequisite for potential therapeutic interventions when such interventions became available in humans.

Our observations recapitulate the clinical utility of exome sequencing in single gene Mendelian disorders, including neurodegeneration with iron accumulation in the brain. In general, the current exome sequencing method provides a high sensitivity for detecting point mutations and small indels but has a low sensitivity for detecting large deletions and triplet nucleotide repeats. In this family, the occurrence of two affected male siblings was highly suggestive of an autosomal recessive or X-linked Mendelian disorder. To maximize the utility of exome sequencing, the selection of appropriate candidate patients based on a combination of clinical, radiographic, and laboratory findings is critical.

In conclusion, two siblings with genetically confirmed GM1 gangliosidosis displayed strikingly similar radiographic progressions. Because paramagnetic signals in the globus pallidus only become apparent relatively late during the disease course, a comprehensive diagnostic approach is necessary for the early identification of affected individuals.

We thank Namiko Saito and Yumi Obayashi for their technical assistance in the preparation of this article. This work was supported by Research on Applying Health Technology (H23-013) and Research into Rare and Intractable Diseases (H23 Jitsuyoka [Nanbyo]-Ippan-003) from the Ministry of Health, Labour and Welfare, Japan.

References

1. Brunetti-Pierri N, Scaglia F. GM1 gangliosidosis: review of clinical, molecular, and therapeutic aspects. *Mol Genet Metab.* 2008;94:391-396.

2. Yang Y, Muzny DM, Reid JG, et al. Clinical whole-exome sequencing for the diagnosis of mendelian disorders. *N Engl J Med.* 2013;369:1502-1511.
3. Pierson TM, Adams DA, Markello T, et al. Exome sequencing as a diagnostic tool in a case of undiagnosed juvenile-onset GM1-gangliosidosis. *Neurology.* 2012;79:123-126.
4. Vieira JP, Conceicao C, Scortenschi E. GM1 gangliosidosis, late infantile onset dystonia, and T2 hypointensity in the globus pallidus and substantia nigra. *Pediatr Neurol.* 2013;49:195-197.
5. De Grandis E, Di Rocco M, Pessagno A, Veneselli E, Rossi A. MR imaging findings in 2 cases of late infantile GM1 gangliosidosis. *AJNR Am J Neuroradiol.* 2009;30:1325-1327.
6. Kosaki R, Takenouchi T, Takeda N, et al. Somatic CTNNB1 mutation in hepatoblastoma from a patient with Simpson-Golabi-Behmel syndrome and germline GPC3 mutation. *Am J Med Genet A.* 2014;164A:993-997.
7. Nishimoto J, Nanba E, Inui K, Okada S, Suzuki K. GM1-gangliosidosis (genetic beta-galactosidase deficiency): identification of four mutations in different clinical phenotypes among Japanese patients. *Am J Hum Genet.* 1991;49:566-574.
8. Aoki S, Okada Y, Nishimura K, et al. Normal deposition of brain iron in childhood and adolescence: MR imaging at 1.5 T. *Radiology.* 1989;172:381-385.
9. Suzuki Y. Chaperone therapy update: Fabry disease, GM1-gangliosidosis and Gaucher disease. *Brain Dev.* 2013;35:515-523.

Novel Overgrowth Syndrome Phenotype Due to Recurrent De Novo *PDGFRB* Mutation

Toshiki Takenouchi, MD[1], Yu Yamaguchi, MD[1], Akiko Tanikawa, MD, PhD[2], Rika Kosaki, MD, PhD[3], Hideyuki Okano, MD, PhD[4], and Kenjiro Kosaki, MD, PhD[5]

Using exome analysis, we identified a novel overgrowth syndrome arising from a mutation in *PDGFRB*, which plays a critical role in growth and differentiation. This entity is characterized by somatic overgrowth, distinctive facial features, hyperelastic and fragile skin, white matter lesions, and neurologic deterioration. *(J Pediatr 2015;166:483-6).*

Overgrowth syndromes are characterized by an accelerated linear growth, either since the fetal period or since birth. More than 10 overgrowth syndromes have been described, and the dysregulation of signaling cascades that control cell growth and differentiation is thought to underlie these disorders.[1] Among these important signaling pathways, whether alterations in the platelet-derived growth factor–NOTCH3 signaling cascade cause a specific syndrome remains uncertain.

Patient Presentation

Patient 1 was born at 39 weeks of gestation without complications. Her birth weight was 3642 g (+1.9 SD), her length was 51.6 cm (+1.6 SD), and her head circumference was 34.6 cm (+1.1 SD). During infancy and childhood, she exhibited normal psychomotor development but had an accelerated linear growth in her height (**Figure 1**, A). At the age of 8 years, she developed a 3-cm tumor on her mandibula, which was removed surgically; the pathology was consistent with myofibroma. At the age of 14 years, her height was 182.1 cm (+4.8 SD), and her weight was 57.6 kg (+0.9 SD), her arm span was 176 cm (+3.6 SD), and her lower segment length was 91 cm (+4.6 SD). Her total hand length was 20.5 cm (+4.6 SD) and her foot length was 27 cm (+4.3 SD). Her facial features included a prominent forehead and supraorbital ridge, mild proptosis and ptosis, downslanting palpebral fissures, a wide nasal bridge, a high columella insertion, a thin upper lip, and a pointed chin. Her skin was hyperelastic, thin, and fragile (**Figure 1**, B1).

At that time, she started to exhibit recurrent episodes of depression and anxiety as well as schizophrenic symptoms, such as blocking or loosening of thought and auditory hallucinations, for which she was treated with risperidone. She had an abnormal cranial shape with protrusion of the posterior fossa and a granular pattern (**Figure 1**, C1 and D1). A fluid-attenuated inversion recovery (FLAIR) magnetic resonance imaging (MRI) of the brain showed hyperintense lesions in the white matter with no evidence of intracranial calcification on computed tomography (**Figure 1**, E1). A chest radiograph showed mild thoracic scoliosis (**Figure 1**, F1).

Patient 2 was born at term with a body weight of 2350 g (−2.1 SD), a length of 49 cm (−0.3 SD), and a head circumference of 31.5 cm (−1.5 SD). She exhibited normal psychomotor development during infancy. Blinded psychological testing using the Stanford-Binet scale (Japanese translation) indicated an IQ of 73 at the age of 5 years and 11 months. This assessment revealed that her short-term memory, in particular, was impaired. Her intellectual disability became more apparent with age, and her IQ was <40 at the age of 13 years. At the age of 17 years, her height was 164.4 cm (restricted by surgically implanted rods in her thoracic vertebrae), her lower segment length was 86 cm (+3.2 SD), her arm span was 171 cm (+2.2 SD), her hand length was 21.0 cm (+5.3 SD), and her foot length was 25.3 cm (+2.4 SD). She had distinctive facial features that were strikingly similar to those of Patient 1: a prominent forehead, proptosis, downslanting palpebral fissures, xanthoma on bilateral upper eyelids, a depressed and wide nasal bridge, thin upper lips, and a pointed chin (**Figure 1**, B2). Her skin was hyperelastic, thin, and fragile but did not have infantile myofibromatosis. She had an abnormal cranial shape with protrusion of the posterior fossa and a granular pattern (**Figure 1**, C2 and D2).

A FLAIR MRI of the brain revealed multifocal hyperintense lesions in the periventricular white matter (**Figure 1**, E2). She underwent a posterior spinal fusion for scoliosis (**Figure 1**, F2) and a secondary cranioplasty for aesthetic

FLAIR	Fluid-attenuated inversion recovery
IBGC	Idiopathic basal ganglia calcification
MRI	Magnetic resonance imaging
PDGFRB	Platelet-derived growth factor receptor B
vSMC	Vascular smooth muscle cell

From the Departments of [1]Pediatrics and [2]Dermatology, Keio University School of Medicine; [3]Division of Medical Genetics, National Center for Child Health and Development; and [4]Department of Physiology and [5]Center for Medical Genetics, Keio University School of Medicine, Tokyo, Japan

Supported by Research on Applying Health Technology (H23-013) from the Ministry of Health, Labour and Welfare, and the Leading Project for Realization of Regenerative Medicine, Support for the Core Institutes for iPS cell research from the Ministry of Education, Culture, Sports, Science, and Technology, Japan. H.O. is a scientific consultant to San Bio, Co Ltd., and Daiichi Sankyo Co, Ltd. The other authors declare no conflicts of interest.

http://dx.doi.org/10.1016/j.jpeds.2014.10.015

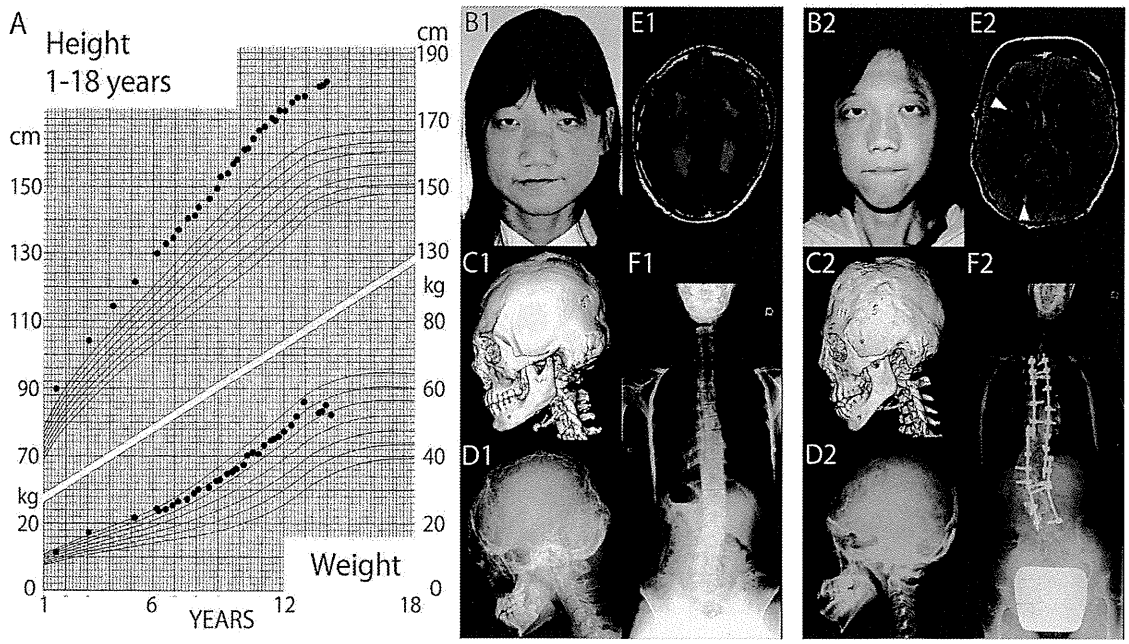

Figure 1. Clinical characteristics of the 2 patients. **A**, **B1**, **C1**, **D1**, **E1**, and **F1**, Images for Patient 1 and **B2**, **C2**, **D2**, **E2**, and **F2**, images for Patient 2 are shown. **A**, A growth chart shows accelerated linear growth for both weight and height. **B1** and **B2**, Facial photographs. **C1** and **C2**, Three-dimensional cranial computed tomography scans showing the protrusion of the posterior fossa. **D1** and **D2**, Skull radiographs showing diffuse granular patterns. **E1** and **E2**, FLAIR brain MRI results showing extensive periventricular white matter lesions (*arrowheads* in **E2**). **F1** and **F2**, Total spine radiographs showing scoliosis.

purposes at the age of 11 years. We previously reported the surgical procedure used in this patient under a presumptive diagnosis of Shprintzen-Goldberg syndrome,[2] but a subsequent mutation analysis for the causative gene, *SKI*, was negative. The family history was noncontributory in both patients (**Figure 2**).

Molecular Analysis

Informed consent from the parents and approval from the local institutional review board were obtained for the molecular studies. DNA was extracted from peripheral blood samples obtained from Patients 1 and 2 and their parents. A whole-exome analysis was performed in Family 1 via use of the MiSeq platform (Illumina, San Diego, California) and SureSelectXT Human All Exon V4 (Agilent Technologies, Santa Clara, California), which provided 10 gigabases per sample, with a mean coverage of 118-fold across the targeted coding regions. More than 98.23% of the regions were covered by >10 reads. Approximately 93 000 variants were identified in Patient 1. The sequencing reads were aligned to the reference human genome sequence (hs37d5) using Burrows-Wheeler Transform,[3] and local realignment around the indels and base quality score recalibration were performed using the Genome Analysis Toolkit[4]; duplicate reads were removed by Picard (http://picard.sourceforge.net).

Nonsynonymous coding variants, splice acceptor and donor site variants, and frameshift coding indels were filtered against dbSNP137, the 1000 Genomes Project (http://www.1000genomes.org/), ESP6500, or the Japanese SNP dataset of 1208 normal individuals (Human Genetic Variation Browser: http://www.genome.med-kyoto-u.ac.jp/SnpDB). A comparison of the exome data for Patient 1 with that of her parents and subsequent Sanger analysis retained platelet-derived growth factor receptor B (*PDGFRB*) as the sole candidate gene in an autosomal-dominant de novo model: a de novo heterozygous missense mutation in exon12 of *PDGFRB* (NM_002609), ie, c.1751C>G p.Pro584Arg, was identified in Patient 1 but not in her parents. No pathologic mutations were identified in any other genes that are associated with overgrowth syndromes, including *FBN1*, *EZH2*, *NSD1*, *PTEN*, *TGFBR1*, and *TGFBR2*. We then sequenced Family 2 and identified the same de novo mutation in Patient 2 but not in the parents (**Figure 2**). Patient 2 did not have whole-exome analysis.

Multiple prediction programs including SIFT, PolyPhen2, and MutationTaster suggested that this amino acid substitution was highly functionally relevant. An evolutional analysis showed that Pro584 and its neighboring amino acids were highly conserved across species. Pro584 is located in the juxtamembrane domain of PDGFRB, which negatively regulates the catalytic activity of cytoplasmic kinases.[5] Within the juxtamembrane domain, the Pro584 maps to the zipper or linker peptide segment, which is thought to correctly align the switching motif in the proper position when changing the autoinhibition status.[6] In addition, autophosphorylation of the neighboring

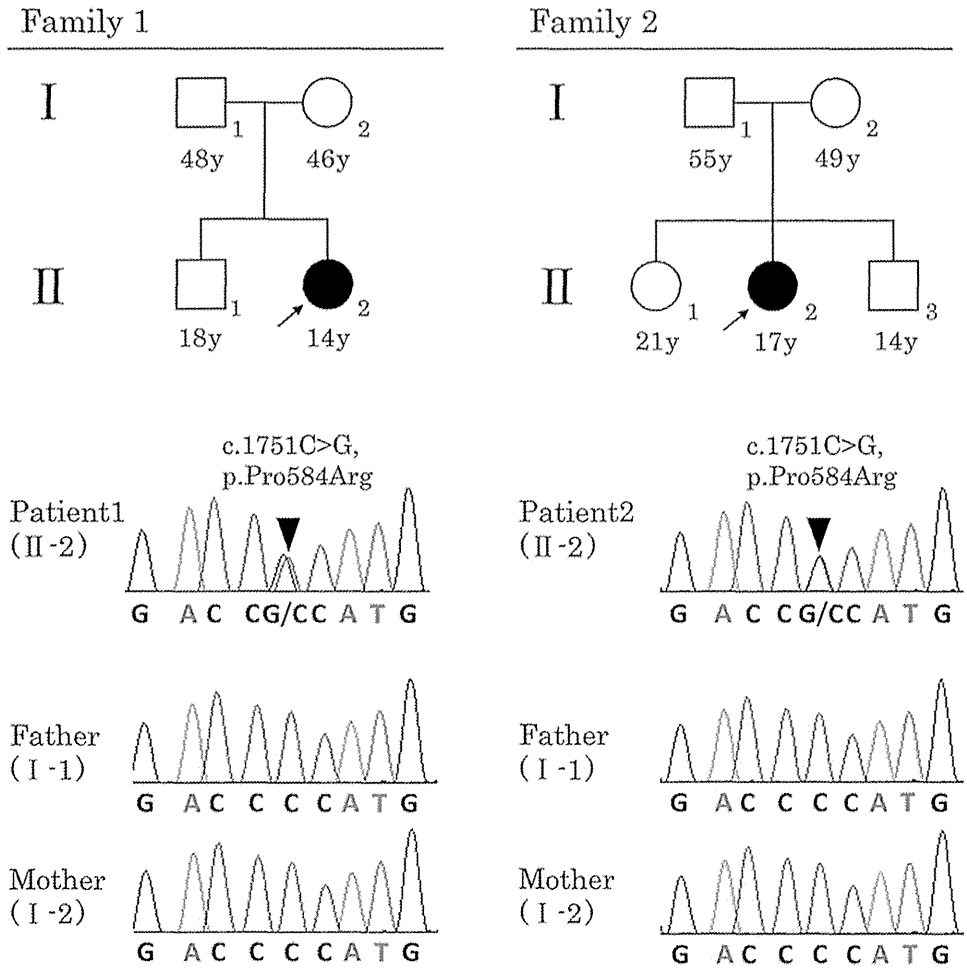

Figure 2. Pedigrees and sequence chromatograms for the 2 families. The pedigrees of Patients 1 and 2 show that no other family members were affected. Sequence chromatograms show that a single nucleotide change, c.1751C>G p.Pro584Arg, was present in Patient 1 and Patient 2 in a heterozygous state. This change was not present in the parents.

tyrosine pair, Tyr579, and Tyr581, is critical in such regulation and serves as docking sites for downstream signal transduction.[7]

Discussion

Through exome sequencing, we have identified a novel form of overgrowth syndrome arising from a *PDGFRB* mutation. The occurrence of the same amino acid substitution in 2 unrelated individuals who presented with a similar phenotype was highly suggestive of a causal relationship, per the recently proposed guidelines for summarizing confidence in variant pathogenicity.[8] Because PDGFRB plays a critical role in the growth and differentiation of cells, the present observation in 2 unrelated patients suggests that the alteration of PDGFRB can lead to the acceleration of linear growth in humans. Besides overgrowth, the characteristic features of this syndrome include characteristic facial features, hyperelastic and fragile skin, white matter lesions, and neurologic deterioration with a delayed onset.

Neurologic deterioration with a delayed onset was conspicuous in the 2 patients. Various neuropsychiatric manifestations, white matter lesions, and calcification in the basal ganglia suggest idiopathic basal ganglia calcification (IBGC).[9] Recently, several families with this condition, but whose members did not exhibit overgrowth, have been reported to carry mutations in *PDGFRB* and *SLA20A2*, a gene encoding a type III Na/Pi transporter.[10] An impaired PDGFRB-Pit-1 pathway is thought to cause calcification in vascular smooth muscle cells (vSMCs) and blood-brain barrier disruption, resulting in delayed intracranial calcification and neuropsychiatric manifestations.[11,12] Because the 2 patients reported here were teenagers, the white matter lesion may represent the early disease stage of this PDGFRB-vSMC pathology.

Infantile myofibroma, a relatively common proliferative fibrous tumor in children, was present in Patient 1. Recently, familial cases of this condition linked to *PDGFRB* and *NOTCH3* mutations were reported.[13,14] The absence of overgrowth or neurologic deterioration and the preservation of

genetic fitness in these familial cases with *PDGFRB* mutations was in contrast to the 2 presently reported patients, suggesting the potential involvement of modifier genes or a second-hit mechanism in the pathogenesis of infantile myofibroma.

The combination of an abnormal cranial shape and scoliosis was characteristic of the 2 presently reported patients with a *PDGFRB* mutation, p.Pro584Arg. No such phenotypic combination was observed in patients with *PDGFRB* mutations other than p.Pro584Arg, who instead exhibited basal ganglia calcification or infantile myofibromatosis.[10,11,13,14] The peculiar phenotypic combination in the 2 patients described herein who exhibit the exact same amino acid substitution may suggest that this substitution exerts specific effects on bone formation, resulting in the unique clinical presentation.

From a molecular standpoint, it is significant that the expression of PDGFRB is directly regulated by NOTCH3.[15] Classically, *NOTCH3* mutations are responsible for cerebral autosomal-dominant arteriopathy with subcortical infarct and leukoencephalopathy, which is characterized by recurrent subcortical ischemic events, vascular dementia, and extensive diffuse white matter lesions.[16] In animals, *Notch3*-knockout mice exhibit a markedly reduced expression of PDGFRB in the vSMCs, where calcification occurs in patients with IBGC.[15] The neurologic deterioration with white matter lesions further suggests that cerebral autosomal-dominant arteriopathy with subcortical infarct and leukoencephalopathy, IBGC, and this novel syndrome share a common cerebral vascular pathology arising from an aberrant NOTCH3-PDGFRB signaling cascade.

PDGFRB is the target molecule of a well-known antileukemic agent, imatinib mesylate.[17] *Pdgfrb*-knockout mice show defects in pericytes, which are necessary for blood-brain barrier formation.[18] Imatinib reverses the increased vascular permeability in such pericyte-deficient mice.[19] These findings suggest a potential therapeutic benefit of imatinib mesylate in this novel syndrome.

In conclusion, the phenotypic features of overgrowth, distinctive facial features, hyperelastic skin, scoliosis, white matter lesions, and neurologic deterioration starting in childhood and adolescence should prompt a novel clinically recognizable syndrome due to the mutation of *PDGFRB*. ■

We thank Chiharu Torii (Center for Medical Genetics, Keio University School of Medicine) for the genetic analysis and the interpretation of the results.

Submitted for publication Mar 9, 2014; last revision received Sep 15, 2014; accepted Oct 3, 2014.

Reprint requests: Kenjiro Kosaki, MD, PhD, Center for Medical Genetics, Keio University School of Medicine, 35 Shinanomachi, Shinjuku-ku, Tokyo 160-8582, Japan. E-mail: kkosaki@z3.keio.jp

References

1. Neylon OM, Werther GA, Sabin MA. Overgrowth syndromes. Curr Opin Pediatr 2012;24:505-11.
2. Watanabe K, Okada E, Kosaki K, Tsuji T, Ishii K, Nakamura M, et al. Surgical treatment for scoliosis in patients with Shprintzen-Goldberg syndrome. J Pediatr Orthop 2011;31:186-93.
3. Li H, Durbin R. Fast and accurate short read alignment with Burrows-Wheeler transform. Bioinformatics 2009;25:1754-60.
4. McKenna A, Hanna M, Banks E, Sivachenko A, Cibulskis K, Kernytsky A, et al. The Genome Analysis Toolkit: a MapReduce framework for analyzing next-generation DNA sequencing data. Genome Res 2010;20:1297-303.
5. Hubbard SR. Juxtamembrane autoinhibition in receptor tyrosine kinases. Nat Rev Mol Cell Biol 2004;5:464-71.
6. Griffith J, Black J, Faerman C, Swenson L, Wynn M, Lu F, et al. The structural basis for autoinhibition of FLT3 by the juxtamembrane domain. Mol Cell 2004;13:169-78.
7. Mori S, Ronnstrand L, Yokote K, Engstrom A, Courtneidge SA, Claesson-Welsh L, et al. Identification of two juxtamembrane autophosphorylation sites in the PDGF beta-receptor; involvement in the interaction with Src family tyrosine kinases. EMBO J 1993;12:2257-64.
8. MacArthur DG, Manolio TA, Dimmock DP, Rehm HL, Shendure J, Abecasis GR, et al. Guidelines for investigating causality of sequence variants in human disease. Nature 2014;508:469-76.
9. Oliveira JR, Spiteri E, Sobrido MJ, Hopfer S, Klepper J, Voit T, et al. Genetic heterogeneity in familial idiopathic basal ganglia calcification (Fahr disease). Neurology 2004;63:2165-7.
10. Lemos RR, Ferreira JB, Keasey MP, Oliveira JR. An update on primary familial brain calcification. Int Rev Neurobiol 2013;110:349-71.
11. Nicolas G, Pottier C, Maltete D, Coutant S, Rovelet-Lecrux A, Legallic S, et al. Mutation of the PDGFRB gene as a cause of idiopathic basal ganglia calcification. Neurology 2013;80:181-7.
12. Wang C, Li Y, Shi L, Ren J, Patti M, Wang T, et al. Mutations in SLC20A2 link familial idiopathic basal ganglia calcification with phosphate homeostasis. Nat Genet 2012;44:254-6.
13. Martignetti JA, Tian L, Li D, Ramirez MC, Camacho-Vanegas O, Camacho SC, et al. Mutations in PDGFRB cause autosomal-dominant infantile myofibromatosis. Am J Hum Genet 2013;92:1001-7.
14. Cheung YH, Gayden T, Campeau PM, Leduc CA, Russo D, Nguyen VH, et al. A recurrent PDGFRB mutation causes familial infantile myofibromatosis. Am J Hum Genet 2013;92:996-1000.
15. Jin S, Hansson EM, Tikka S, Lanner F, Sahlgren C, Farnebo F, et al. Notch signaling regulates platelet-derived growth factor receptor-beta expression in vascular smooth muscle cells. Circ Res 2008;102:1483-91.
16. Joutel A, Corpechot C, Ducros A, Vahedi K, Chabriat H, Mouton P, et al. Notch3 mutations in CADASIL, a hereditary adult-onset condition causing stroke and dementia. Nature 1996;383:707-10.
17. Apperley JF, Gardembas M, Melo JV, Russell-Jones R, Bain BJ, Baxter EJ, et al. Response to imatinib mesylate in patients with chronic myeloproliferative diseases with rearrangements of the platelet-derived growth factor receptor beta. N Engl J Med 2002;347:481-7.
18. Daneman R, Zhou L, Kebede AA, Barres BA. Pericytes are required for blood-brain barrier integrity during embryogenesis. Nature 2010;468:562-6.
19. Armulik A, Genove G, Mae M, Nisancioglu MH, Wallgard E, Niaudet C, et al. Pericytes regulate the blood-brain barrier. Nature 2010;468:557-61.

J Clin Immunol
DOI 10.1007/s10875-015-0127-7

ASTUTE CLINICIAN REPORT

X-Linked Agammaglobulinemia Associated with B-Precursor Acute Lymphoblastic Leukemia

Akihiro Hoshino · Yusuke Okuno · Masahiro Migita · Hideki Ban · Xi Yang · Nobutaka Kiyokawa · Yuichi Adachi · Seiji Kojima · Osamu Ohara · Hirokazu Kanegane

Received: 25 November 2014 / Accepted: 2 January 2015

Abstract X-linked agammaglobulinemia (XLA) is clinically characterized by reduced number of peripheral B cells and diminished levels of serum immunoglobulins, and caused by a mutation in the *Bruton's tyrosine kinase* (*BTK*) gene, which play a pivotal role in signal transduction of pre-B-cell receptor (BCR) and BCR. B-cell precursor acute lymphoblastic leukemia (BCP-ALL) is the most common malignancy in children, and it may be associated with gene alterations that regulate B-cell development. Here we described a first case of XLA associated BCP-ALL. The whole-exome sequencing revealed a somatic mutation in *MLL2* in the sample from the onset of BCP-ALL. This study suggests that the alterations of *BTK* and *MLL2* synergistically function as leukemogenesis.

A. Hoshino · X. Yang · Y. Adachi
Department of Pediatrics, Graduate School of Medicine and Pharmaceutical Sciences, University of Toyama, Toyama, Japan

Y. Okuno · S. Kojima
Department of Pediatrics, Nagoya University Graduate School of Medicine, Nagoya, Japan

M. Migita · H. Ban
Department of Pediatrics, Japanese Red Cross Kumamoto Hospital, Kumamoto, Japan

N. Kiyokawa
Department of Pediatric Hematology and Oncology Research, National Research Institute for Child Health and Development, Tokyo, Japan

O. Ohara
Department of Technology Development, Kazusa DNA Research Institute, Kisarazu, Japan

H. Kanegane (✉)
Department of Pediatrics and Developmental Biology, Graduate School of Medical and Dental Sciences, Tokyo Medical and Dental University, 1-5-45 Yushima, Bunkyo-ku, Tokyo 113-8519, Japan
e-mail: hkanegane.ped@tmd.ac.jp

Published online: 16 January 2015

Keywords Acute lymphoblastic leukemia · Bruton's tyrosine kinase · *MLL2* · X-linked agammaglobulinemia

Introduction

X-linked agammaglobulinemia (XLA) is a primary immunodeficiency disease characterized by lack of peripheral B cells and low levels of serum immunoglobulins; it is caused by a mutation of the gene encoding *Burton's tyrosine kinase* (*BTK*) [1]. BTK functions downstream of multiple receptors in various hematopoietic cells. It also plays a pivotal role in signal transduction of pre-B-cell receptor (BCR) and BCR [1]. The activation of pre-BCR and BCR, which results in signal cascade of downstream molecules, is required for the development of B cells, and *BTK* alterations impede the development of pro-B cells beyond the early pre-B-cell stage to the later stage of pre-B cells [2]. Indeed, XLA patients show severely reduced numbers of mature B cells, whereas pro-B cells are present in the bone marrow of patients with XLA in normal or increased numbers [2]. B-cell precursor acute lymphoblastic leukemia (BCP-ALL) is the most common malignancy in children, and its pathogenesis is explained by the impairment of lymphoid development and normal cellular functions, including cell cycle regulation, tumor suppression and lymphoid signaling [3]. Genome-wide analysis has revealed alterations in genes that regulate B-cell development in more than two-thirds of BCP-ALL patients, including *PAX5*, *TCF3*, *EBF1*, *LEF1* and *IKZF1* [4]. Recently, germline *PAX5* mutations were identified in familial leukemias [5]. Given that impairment of lymphoid development is related to leukemogenesis, there is a possibility that XLA patients have increased susceptibility to BCP-ALL. This is an initial report of a BCP-ALL patient associated with XLA, for whom whole-exome sequencing revealed an acquired mutation in *MLL2*. This study was approved by the ethics board of the University of Toyama.

Material and Methods

Patient Report

The patient was a 10-year-old boy, who had contracted pneumococcal meningitis at the age of 3 years and had suffered from recurrent bacterial infections including otitis media. The family history was unremarkable. The percentage of B cells and serum immunoglobulin levels were markedly reduced (B cells 0.3 %, IgG 7 mg/dl, IgA 3 mg/dl, IgM 30 mg/dl). At the age of 6 years, the patient was diagnosed as having XLA with a *BTK* c.1051A>G (p.R307G) missense mutation (Fig. 1a), the pathogenicity of which has been reported in a public database (SH2base: http://bioinf.uta.fi/SH2base/BTK.html). Regular intravenous immunoglobulin (IVIG) replacement therapy was started. When he was 10 years old, a routine hematological study incidentally disclosed lymphoblasts in the peripheral blood. His white blood cell count was 7.0×10^9/L with 15.0 % lymphoblasts, hemoglobin was 12.0 g/dL and platelet count was 185,000/μL. Bone marrow aspiration revealed hypercellular marrow, with 96.2 % lymphoblasts. Flow cytometry revealed that the lymphoblasts were positive for CD10 (99.7 %), CD19 (99.7 %), CD22 (97.9 %), cy-CD79a (96.4 %), CD34 (99.8 %) and cy-TdT (95.4 %) and HLA-DR (98.8 %) and negative for CD20, cy-Igμ chain, Igμ chain, Igκ chain, Igλ chain, and all of the T-lineage and myeloid markers except CD2 (99.2 %). The karyotype was normal, and real-time polymerase chain reaction detected no major *BCR-ABL1*, minor *bcr-abl1*, *TCF3-PBX*, *MLL-AF4*, *MLL-AF9*, *MLL-ENL*, *ETV6-RUNX1* and *SIL-TAL1* fusion. The patient was diagnosed with BCP-ALL, and received chemotherapy according to the Tokyo Children's Cancer Study Group (TCCSG) ALL L04-16 high-risk group protocol. He had a good clinical course, and the chemotherapy was just finished. No severe complications occurred except for one episode of febrile neutropenia.

Whole-Exome Sequencing

Whole-exome sequencing was performed to identify secondary genetic events. Paired leukemia cell DNA from bone marrow cells at diagnosis and control DNA from peripheral blood mononuclear cells in remission were analyzed. Exome capture was carried out using a TruSeq Exome Enrichment Kit (Illumina) according to the manufacturer's protocol. Massively-parallel sequencing was performed using a HiSeq 1500 platform (Illumina) with 100 bp-paired-end reads. Sequence reads were aligned to the human reference genome using Burrows-Wheeler Aligner. SAMtools, Genome Analysis Toolkit (GATK) and Picard Tools were used for downstream processing and variant calling. Calls with a read coverage<5×were filtered out, resulting in>96 % coverage for the entire target region. Detected tumor-specific candidate variants were further filtered using dbSNP137, Human Genetic Variation Database (HGVD; http://www.genome.med.kyoto-u.ac.jp/SnpDB/) and our in-house SNP database. As a result, six tumor-specific variants were identified (Table 1). Among these variants, a *MLL2* c.8740delC (p.H2914fs) mutation was considered a driver mutation, because it is an inactivating mutation and the gene is reported to be recurrently inactivated in diffuse large B-cell lymphoma (DLBCL) [6, 7]. For the other five variants, we performed an extensive literature search but could not find reports supporting their driver role. We also evaluated 237 novel germline nonsynonymous variants that were not registered in SNP databases. However, even with knowledge from genome-wide association studies of

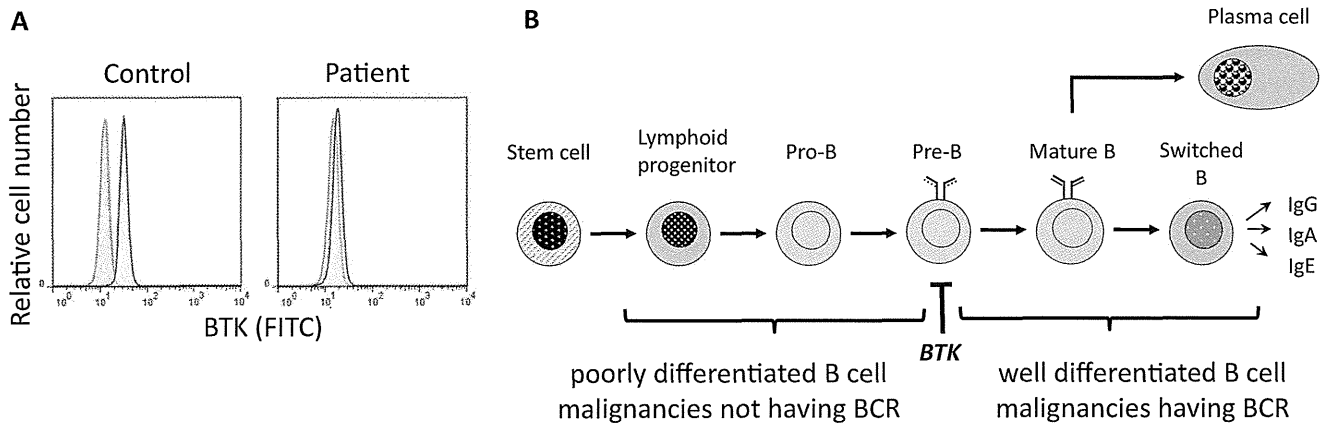

Fig. 1 BTK expression and its role in leukemogenesis. **a** Intracellular BTK expression in $CD14^+$ monocytes evaluated by flow cytometry (BD LSRFortessa™ Cell Analyzer, BD Biosciences, San Diego, CA). Black histograms indicate BTK expression (clone 10E10, OriGene Technologies, Inc., Rockville, MD), and Gray histograms indicate isotype control. BTK expression in the patient was reduced compared with that in a normal control. **b** Two different roles of *BTK* in the development of B-cell malignancies. Absence of BTK-dependent BCR signals may promote the development of poorly differentiated B-cell malignancies. Activated BTK-dependent BCR signals promote the development of well-differentiated B-cell malignancies

Table 1 Somatic variants detected in leukemia cells

Gene	Effect	CDS change	Protein change	Genotype	Chromosome	Cancer tissue in COSMIC*
GLT25D2	Missense	c.1019G>T	p.Gly340Val	hetero	1q25	none
DNAH14	Missense	c.2810C>A	p.Thr937Lys	hetero	1q42	endometrium
DAPK1	Missense	c.3688C>A	p.Leu1230Ile	hetero	9q34.1	endometrium, large intestine
MLL2	Frameshift	c.8740delC	p.His2914Thrfs	hetero	12q12-q14	cervix, urinary tract, endometrium, large intestine, lung, hematopoietic and lymphoid
COG8	Missense	c.284A>G	p.Glu95Gly	hetero	16q22.1	none
ALKBH6	Missense	c.16A>G	p.Met6Val	hetero	19q13.12	none

*Cancer tissue: > 5 % have the mutation in the Catalogue of Somatic Mutations in Cancer database

CDS coding sequence, *COSMIC* catalogue of somatic mutations in cancer

ALL and the Catalogue of Somatic Mutations in Cancer (COSMIC) database [8], we could not identify possibly pathogenic variants except the *BTK* c.1051A>G mutation.

Discussion

It is tempting to hypothesize that a germline *BTK* mutation and an acquired *MLL2* mutation are sufficient to cause a leukemic transformation in B lymphocyte precursors with defective maturation. The development of leukemia cells was arrested just before the stage that required BTK. Previous studies identified that several BCP-ALL cells have aberrant expression of BTK caused by somatic mutations or aberrant transcription of *BTK* [9]. It is noteworthy that many of these observations were identified in *MLL*-rearranged ALL [9]. *MLL2* is a histone methyltransferase and its impaired function results in aberrant DNA methylation. Haploinsufficiency of *MLL2* is sufficient to drive molecular pathogenesis. A heterozygous germline mutation results in a characteristic systemic disorder named Kabuki syndrome [10], and the somatic *MLL2* mutation observed in DLBCL is also heterozygous [6, 7]. However, the fact that our current knowledge about gene mutations remains markedly limited and the possibility of the existence of a fusion gene that we have not tested weaken the hypothesis.

Of greatest interest was that BCP-ALL with an *MLL2* mutation occurred in a *BTK*-deficient patient whereas BTK inhibitor is effective in some DLBCL patients [11], most likely having *MLL2* mutation. According to our findings and previous reports, we suggest two different roles of *BTK* in the pathogenesis of B-cell malignancies according to the degree of their differentiation (Fig. 1b). Firstly, constitutively or aberrantly activated BTK-dependent signals from BCR can promote the development of well-differentiated B-cell malignancies [12, 13]. Secondly, absence of BTK-dependent signals, which result in developmental arrest of B cells, can promote the development of poorly differentiated B-cell malignancies such as BCP-ALL. Our report provides the first evidence of a germline *BTK* mutation and an acquired *MLL2* mutation affecting leukemogenesis, as well as a new insight into germline mutations in leukemia development.

Acknowledgments This study was supported by grants from the Ministry of Health, Labour, Welfare of Japan. We thank Chikako Sakai and Hitoshi Moriuchi for their excellent technical assistance. This study is dedicated to the late Dr. Toshio Miyawaki.

References

1. Tsukada S, Saffran DC, Rawlings DJ, Parolini O, Allen RC, Klisak I, et al. Deficient expression of a B cell cytoplasmic tyrosine kinase in human X-linked agammaglobulinemia. Cell. 1993;72:279–90.
2. Nomura K, Kanegane H, Karasuyama H, Tsukada S, Agematsu K, Murakami G, et al. Genetic defect in human X-linked agammaglobulinemia impedes a maturational evolution of pro-B cells into a later stage of pre-B cells in the B-cell differentiation pathway. Blood. 2000;96:610–7.
3. Inaba H, Greaves M, Mullighan CG. Acute lymphoblastic leukaemia. Lancet. 2013;381:1943–55.
4. Mullighan CG, Su X, Zhang J, Radtke I, Phillips LA, Miller CB, et al. Deletion of IKZF1 and prognosis in acute lymphoblastic leukemia. N Engl J Med. 2009;360:470–80.
5. Shah S, Schrader KA, Waanders E, Timms AE, Vijai J, Miething C, et al. A recurrent germline PAX5 mutation confers susceptibility to pre-B cell acute lymphoblastic leukemia. Nat Genet. 2013;45:1226–31.
6. Morin RD, Mendez-Lago M, Mungall AJ, Goya R, Mungall KL, Corbett RD, et al. Frequent mutation of histone-modifying genes in non-Hodgkin lymphoma. Nature. 2011;476:298–303.
7. Pasqualucci L, Trifonov V, Fabbri G, Ma J, Rossi D, Chiarenza A, et al. Analysis of the coding genome of diffuse large B-cell lymphoma. Nat Genet. 2011;43:830–7.
8. Urayama KY, Chokkalingam AP, Manabe A, Mizutani S. Current evidence for an inherited genetic basis of childhood acute lymphoblastic leukemia. Int J Hematol. 2013;97:3–19.
9. Feldhahn N, Río P, Soh BN, Liedtke S, Sprangers M, Klein F, et al. Deficiency of Bruton's tyrosine kinase in B cell precursor leukemia cells. Proc Natl Acad Sci U S A. 2005;102:13266–71.

10. Ng SB, Bigham AW, Buckingham KJ, Hannibal MC, McMillin MJ, Gildersleeve HI, et al. Exome sequencing identifies MLL2 mutations as a cause of Kabuki syndrome. Nat Genet. 2010;42:790–3.
11. Wilson WH, Gerecitano JF, Goy A, de Vos S, Kenkre VP, Barr PM, et al. The Bruton's tyrosine kinase (BTK) inhibitor, ibrutinib (PCI-32765), has preferential activity in the ABC subtype of relapsed/refractory de novo diffuse large B-cell lymphoma (DLBCL): interim results of a multicenter, open-label, phase 2 study. Blood. 2012;120:686 (abstract).
12. Aalipour A, Advani RH. Bruton tyrosine kinase inhibitors: a promising novel targeted treatment for B cell lymphomas. Br J Haematol. 2013;163:436–43.
13. de Rooij MF, Kuil A, Geest CR, Eldering E, Chang BY, Buggy JJ, et al. The clinically active BTK inhibitor PCI-32765 targets B-cell receptor- and chemokine-controlled adhesion and migration in chronic lymphocytic leukemia. Blood. 2012;119:2590–4.

Acta Derm Venereol 2015; 95: 98–99

SHORT COMMUNICATION

Merkel Cell Polyomavirus-positive Merkel Cell Carcinoma in a Patient with Epidermodysplasia Verruciformis

Yuki Mizuno[1], Genichi Kato[1], En Shu[1], Hidenori Ohnishi[2], Toshiyuki Fukao[2], Osamu Ohara[3,4], Hitomi Fukumoto[5], Harutaka Katano[5] and Mariko Seishima[1]*

*Departments of [1]Dermatology and [2]Pediatrics, Graduate School of Medicine, Gifu University, 1-1 Yanagido, Gifu 501-1194, [3]Laboratory for Immunogenomics, RIKEN Research Center for Allergy and Immunology, Yokohama, Kanagawa, [4]Department of Human Genome Research, Kazusa DNA Research Institute, Kisarazu, Chiba, and [5]Department of Pathology, National Institute of Infectious Diseases, Tokyo, Japan. *E-mail: marikoseishima@yahoo.co.jp*

Accepted Apr 2, 2014; Epub ahead of print Apr 7, 2014

Epidermodysplasia verruciformis (EV) is a rare autosomal recessive disease characterised by abnormal susceptibility to disease-specific human papillomaviruses (HPVs), possibly due to suppressed cellular innate immunity. *EVER1/TMC6* or *EVER2/TMC8* gene mutations are often found in EV (1). All patients with EV usually have similar skin lesions from their childhood, involving disseminated flat warts or pityriasis versicolor. Elderly patients with EV have a high risk of developing carcinomas *in situ* and invasive squamous cell carcinoma (SCC) associated with HPV infections, mainly on sun-exposed skin. On the other hand, Merkel cell polyomavirus (MCPyV) is detected in most Merkel cell carcinomas (MCC) (2), which arise from Merkel cells, neuroendocrine cells in the skin. We present here a rare occurrence of $MCPyV^+$ MCC in a patient with EV.

CASE REPORT

An 82-year-old Japanese man with chronic obstructive pulmonary disease and repeated occurrence of bacterial pneumonia noticed a rapidly growing tumour on his left cheek one month earlier. He had noticed flat verruous papules and brown macules on the neck, face and chest in his twenties. He had a 25-year-history of various skin conditions, including seborrhoeic keratosis, actinic keratosis, Bowen's disease, basal cell carcinoma, and SCC on the skin of the scalp, face, and neck that had been treated with various surgical operations and cryotherapy. Infection with HPV 16 was detected when the patient was evaluated for Bowen's disease and SCC. Although we recommended check-up every 6 months for recurrence of SCC and new skin neoplasms, he did not visit us regularly.

On the patient's return 2 years later, a hard, pink tumour (3.5 × 3.3 cm in size; height 1.4 cm) was noted on the left cheek. At the base of the tumour, there was a hard induration area (size 4 × 6 cm) with undefined borders (Fig. 1a). In addition, the left cervical lymph node was swollen. Histological study of the biopsy specimen from the tumour showed massive tumour nests from the dermis to the subcutaneous tissue, which were composed of small, oval, basophilic tumour cells with poor cytoplasm (Fig. 1b, d). Several tumour cells appeared to be in stages of mitosis. Immunostaining showed that the tumour cells were positive for cytokeratin 20 (Fig. 1c), synaptophysin, chromogranin A, and AE1/AE3, but negative for cytokeratin 7 and thyroid-transcription factor-1 (TTF-1). The MIB-1/Ki-67 labelling index was 75%, indicating the proliferation of tumour

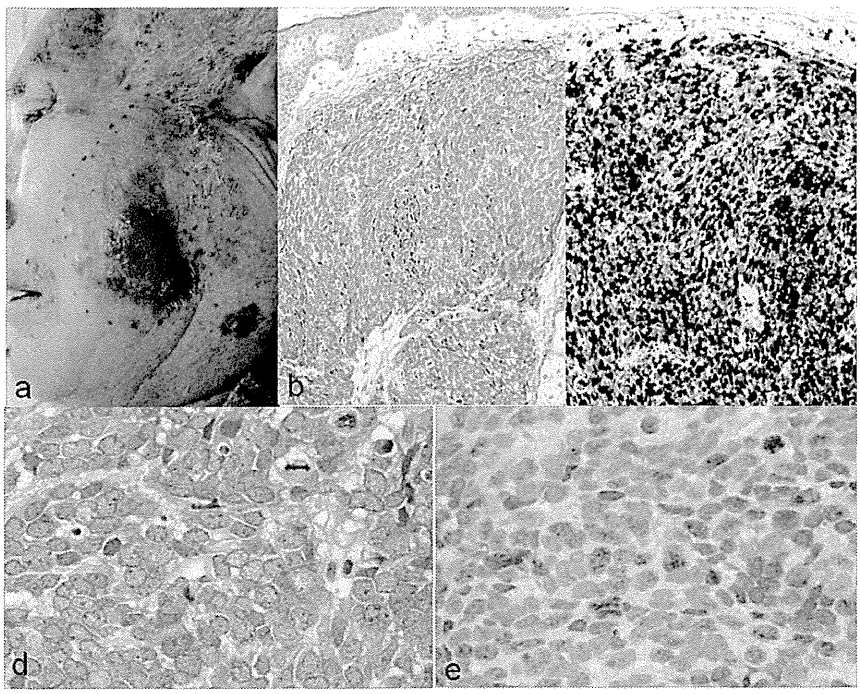

Fig. 1. A large tumour on the left cheek (a). Tumour nest with oval atypical cells from the dermis to the subcutaneous tissue (H&E stain, original magnification; b: × 100 and d: × 400). Immunopathological findings by MIB-1/Ki-67 (c) and Merkel cell polyomavirus large T-antigen (e) (c: × 100 and e: × 400).